Typeset using LaTeX **twocolumn** style in AASTeX63

Facilities: VLT:Yepun (MUSE); OANSPM:2.1m (Mezcal); Keck (HIRES) Draft version September 8, 2019

Raman mapping of photodissociation regions in Orion

William J. Henney[1]

[1]*Instituto de Radioastronomía y Astrofísica, Universidad Nacional Autónoma de México, Apartado Postal 3-72, 58090 Morelia, Michaoacán, Mexico*

Abstract

I show that the broad Raman-scattered wings of Hα can be used to map neutral gas illuminated by high-mass stars in star forming regions. The near wings ($\Delta\lambda \approx \pm 10$ Å) trace neutral hydrogen columns of about 5×10^{20} cm^{-2}, while the farther wings ($|\Delta\lambda| > 30$ Å) trace columns of about 5×10^{21} cm^{-2}. Absorption features in the pseudo-continuum at 6633 and 6664 Å correspond to neutral oxygen far-ultraviolet absorption lines at 1027.43 Å and 1028.16 Å.

Keywords: Atomic physics; Radiative transfer; Photodissociation regions

1. INTRODUCTION

Raman scattering is the inelastic analog of Rayleigh scattering by atoms or molecules. Both processes begin with a radiation-induced transition of an electron to a virtual bound state (non-eigenstate). In Rayleigh scattering, the electron returns to its original state, resulting in the radiation being re-emitted with its original frequency (elastic scattering). In Raman scattering, on the other hand, the electron undergoes a transition to a different excited state, resulting in radiation being re-emitted at a much lower frequency. Recently, Dopita et al. (2016) identified exceedingly broad wings to the Hα 6563 Å line in the Orion Nebula and a number of H II regions in the Magellanic Clouds, which they ascribe to Raman scattering of ultraviolet radiation in the vicinity of the Lyβ 1025 Å transition. Raman scattering in astrophysical sources was first identified in symbiotic stars (Schmid 1989), where FUV O VI emission lines at 1032 and 1038 Å produce broad emission features at 6827 and 7088 Å. This illustrates a curious feature of Raman scattering (Nussbaumer et al. 1989): the relative width $\Delta\lambda/\lambda$ of spectral features is amplified by a factor $\lambda(\mathrm{H}\alpha)/\lambda(\mathrm{Ly}\beta) \approx 6.4$ when passing from the FUV to the optical domain.

Dopita et al. (2016) propose that the Raman wings form at the transition zone near the ionization fronts in H II regions. However, the total neutral hydrogen column through the ionization front can be no more than about $10/\sigma_0 \approx 2 \times 10^{18}$ cm^{-2}, where $\sigma_0 \approx 6.3 \times 10^{-18}$ cm^2 is the ground-state hydrogen photoionization cross section at threshold (Osterbrock & Ferland 2006). The Raman scattering cross section at wavelengths responsible for the observed wings is much lower than this: $\sigma_{\mathrm{Raman}} \sim 10^{-21}$ cm^2 (Chang et al. 2015), meaning that the Raman scattering optical depth through the ionization front is only of order 0.001. A vastly larger column density of neutral hydrogen ($\approx 10^{21}$ cm^{-2}) is available in the photodissociation region (PDR) outside the ionization front, so it is more likely that Raman scattering will occur there instead, so long as there is sufficient far ultraviolet radiative flux.

This paper is organized as follows. § 2 recapitulates the basic theory of Raman scattering, concentrating on the wavelength transformation from the FUV domain around Lyβ to optical domain around Hα. In addition, polynomial fits are provided to the wavelength dependence of the total (Rayleigh plus Raman) scattering cross section and the Raman Hα branching ratio. § 3 then presents archival VLT-MUSE integral field spectroscopy of the Orion Nebula, which allows the broad Hα wings to be spatially mapped in unprecedented detail and compared with other tracers of ionized and neutral zones in the nebula. Two components of the O I UV resonance multiplet $2p^4\ ^3P \rightarrow 3d\ ^3D^o$ are detected as absorption features at 6633 and 6664 Å against the Hα Raman wings. § 4 presents archival Keck-HIRES slit spectroscopy, which shows the profile of the 6664 Å absorption line with an effective velocity resolution of 1 km s^{-1}. § 5 discusses the implications of these results for the structure and dynamics of the PDRs in Orion, together with the prospects for using Raman spectral mapping as a diagnostic tool in the study of other high-mass star formation regions.

2. RAMAN SCATTERING THEORY

When a photon is Raman-scattered from the vicinity of Lyβ (UV domain) to the vicinity of Hα (optical domain) its wavelength is transformed from λ_1 to λ_2. Intervals in frequency ($\nu = c/\lambda$) or wavenumber ($\tilde{\nu} = 1/\lambda$) space are conserved between the two domains. For example the wavenumber dis-

w.henney@irya.unam.mx

Table 1. FUV/optical wavelength equivalencies for Raman scattering

Ion	Transition	$J_i \rightarrow J_k$	λ_1, Å	$\tilde{\nu}_1$, cm^{-1}	$\Delta\tilde{\nu}$, cm^{-1}	$\tilde{\nu}_2$, cm^{-1}	λ_2, Å	$\lambda_{\rm air}$, Å
			.... Lyβ, $n = 1$			.....	Hα, $n = 2$	.....
H I	$ns\ ^2$S $\rightarrow$ 3p ^{2}P	$\frac{1}{2} \rightarrow \frac{1}{2}, \frac{3}{2}$	1025.72220	97492.283	0.000	15233.329	6564.553	6562.740
O I	2s^{2}2p^4 ^{3}P $\rightarrow$ 2s^{2}2p^3(^{4}S)3d ^{3}D^o	0 $\rightarrow$ 1	1028.15729	97261.383	−230.900	15002.429	6665.587	6663.747
		1 $\rightarrow$ 1	1027.43139	97330.100	−162.183	15071.146	6635.196	6633.364
		1 $\rightarrow$ 2	1027.43077	97330.159	−162.124	15071.205	6635.170	6633.338
		2 $\rightarrow$ 1	1025.76339	97488.369	−3.914	15229.415	6566.240	6564.427
		2 $\rightarrow$ 2	1025.76276	97488.429	−3.854	15229.475	6566.215	6564.401
		2 $\rightarrow$ 3	1025.76170	97488.530	−3.753	15229.576	6566.171	6564.358

placement from the H I line center can be written in two ways:

$$\Delta\tilde{\nu} = \tilde{\nu}_1 - \tilde{\nu}(\mathrm{Ly}\beta) = \tilde{\nu}_2 - \tilde{\nu}(\mathrm{H}\alpha)\,, \tag{1}$$

from which it follows that

$$\lambda_2 = \left(\frac{1}{\lambda(\mathrm{H}\alpha)} + \frac{1}{\lambda_1} - \frac{1}{\lambda(\mathrm{Ly}\beta)}\right)^{-1}\,. \tag{2}$$

The wavelengths λ(Lyβ) and λ(Hα), together with their corresponding wavenumbers, are given in Table 1 (all wavelengths are on the vacuum scale unless otherwise noted). For both lines, a weighted average over the 3p ^{2}P$_{1/2}$ and 3p ^{2}P$_{3/2}$ upper levels is used, assumed to be populated according to their statistical weights, with individual component wavelengths obtained from Tab. XXVIII of Mohr et al. (2008). Note that the electric dipole selection rules mean that only 3p $\rightarrow$ 2s transitions contribute to Hα in the Raman scattering context. The wavelength is therefore slightly shorter than the value obtained for the Hα recombination line, which includes additional contributions from 3s $\rightarrow$ 2p and 3d $\rightarrow$ 2p. The shift is of order −0.05 Å or −2 km s^{-1} with respect to the Case B results reported in Tab. 6a of Clegg et al. (1999).

Also listed in Table 1 are the Raman transformations $\lambda_1 \rightarrow \lambda_2$ for the rest wavelengths of transitions between the ground 2s^{2}2p^4 ^{3}P term of neutral ^{16}O and the excited 2s^{2}2p^{3}3d ^{3}D^o term. The O I data is obtained from highly accurate laser metrology (Ivanov et al. 2008; Marinov et al. 2017), with a precision of 0.08 cm^{-1} or better. The fine structure splitting between the J_k levels of the excited term ($\sim$ 0.1 cm^{-1}) is much smaller than that between the J_i levels of the ground term ($\sim$ 100 cm^{-2}), so that the 6 transitions fall into 3 well-separated groups. The three transitions from the lowest energy $J_i = 2$ level are very close to Lyβ ($\Delta\tilde{\nu} \approx 4$ cm^{-1}), whereas the two transitions from $J_i = 1$ ($\Delta\tilde{\nu} \approx 162$ cm^{-1}) and the single transition from $J_i = 0$ ($\Delta\tilde{\nu} \approx 231$ cm^{-1}) lie increasingly to the red. The corresponding wavelengths in the optical domain, λ_2, are therefore on the red side of Hα. The final column of the table uses STP refractive indices (Greisen et al. 2006) to convert λ_2 to air wavelengths, $\lambda_{\rm air}$, for ease of comparison with ground-based optical spectroscopy. The resultant wavelength is 6663.747 Å for the line from $J_i = 0$, with an uncertainty of about 0.004 Å, which is much smaller than typical observational precision (for instance, 0.07 Å for a very high resolution spectrograph with resolving power of $R = 10^5$). The two lines from $J_i = 1$, with a separation of 0.028 Å, will always be blended in observations, giving a mean wavelength of 6633.347 Å (assuming the upper levels are distributed according to statistical weight $2J_k + 1$). Similarly, the three lines from $J_i = 2$ have a mean wavelength of 6564.386 Å, but this is so close to Hα (corresponding to a Doppler shift of 75 km s^{-1}) that it would be very difficult to observe.

The total cross-section for the non-resonant 1s $\rightarrow$ 3p transition in H^0 is calculated in § 2 of Chang et al. (2015) from second order time-dependent perturbation theory. Results are presented in the upper panel of Figure 1 of that paper in terms of a Doppler velocity factor ΔV_1, which in the notation of the current paper is

$$\Delta V_1 = c\left(\frac{\lambda_1}{\lambda(\mathrm{Ly}\beta)} - 1\right)\,. \tag{3}$$

The observed Raman-scattered wings of Hα that are analyzed below are typically within $\Delta\lambda_2 \sim \pm 100$ Å of the line core. It is therefore convenient to define a dimensionless wavelength in the optical domain as

$$x = \frac{\lambda_2 - \lambda(\mathrm{H}\alpha)}{100\ \text{Å}}\,, \tag{4}$$

which corresponds to $x \approx \Delta V_1/714$ km s^{-1} in the FUV domain. The total cross section in the range $0.4 < |x| < 2.3$ can then be fit as follows:

$$\frac{\sigma}{10^{-21}\ \mathrm{cm}^2} = \begin{cases} 0.2186x^{-2} - 0.0344x^{-1} - 0.0054 & \text{if } x < 0 \\ 0.2367x^{-2} - 0.0187x^{-1} + 0.0041 & \text{if } x > 0 \end{cases} \tag{5}$$

Note that separate fits are given for the blue ($x < 0$) and red ($x > 0$) wings of Hα since the cross section, although approximately Lorentzian, is not exactly symmetric, being stronger on the blue side (by about 10% for $x = \pm 1$).

The fraction of all 1s → 3p excitations that result in Raman scattering to an optical photon is given by the branching ratio, $f_{\mathrm{H}\alpha}$, with the remaining fraction, $1 - f_{\mathrm{H}\alpha}$, resulting in elastic Rayleigh scattering in which the photon remains in the FUV domain. The results for $f_{\mathrm{H}\alpha}$ are also shown in Figure 1 of Chang et al. (2015) and can be fit as follows in the range $|x| < 5$:

$$f_{\mathrm{H}\alpha} = 0.2238 + 0.0363x + 0.0024x^2 \ . \quad (6)$$

The relative accuracy of all these fits is better than 1% within the stated range (corresponding to $\sigma \approx 10^{-22}\,\mathrm{cm}^2$ to $10^{-21}\,\mathrm{cm}^2$), which is perfectly adequate for the purposes of this paper. Note that the branching ratio increases with x, which means that the product $\sigma f_{\mathrm{H}\alpha}$ is stronger on the red side of Hα.

3. SPECTRAL MAPPING OF RAMAN WINGS

The 6633 Å and 6664 Å lines are clearly detected in the MUSE spectra as absorption features against the pseudo-continuum of the broad Hα wings (see Fig XX), although the latter is blended with a Ni II emission line at 6666.8 Å. This is further proof of the Raman scattering nature of the wings.

MUSE (Bacon et al. 2010) observations of the Orion Nebula (Weilbacher et al. 2015; Mc Leod et al. 2015).

The bands are chosen to avoid the stronger sky lines (e.g., 6498 Å) and nebula lines (e.g.,), but some weak line contamination remains, as listed in the last column of Table 2.

4. HIGH-RESOLUTION SPECTROSCOPY OF RAMAN-SCATTERED O I 1028 Å

Keck HIRES spectra described in Henney & O'Dell (1999) and Bally et al. (2000). The spectrum I use is of HH 529 base region in Orion South. Published results from these data have concentrated on strong nebular lines, but here I use a small section of the spectrum in the range 6660 Å to 6670 Å for reasons which will become apparent.

5. DISCUSSION

The effective resolving power of the optical spectrograph is multiplied by 6.4 for the FUV domain.

The O I lines should be in absorption in the spectrum seen by the Raman scatterers.

Salgado et al. (2016) had found low dust cross-section in Orion Bar PDR, but there are loopholes. First, they assume plane-parallel geometry with exactly edge-on viewing angle, while in reality it is a roughly cylindrical filament. Second, they ignore scattering, see Watson et al. (1998).

Non-equilibrium PDRs (Stoerzer & Hollenbach 1998; Bertoldi & Draine 1996). Recent models from Bron et al. (2018).

C I emission from non-steady PDRs (Stoerzer et al. 1997) (fine structure lines, but maybe optical lines would be similar). Escalante et al. (1991) model the far-red [C I] line as recombination of C^+.

O VI 1037.62, 1031.93 absorption line in wind. No evidence for a blue absorption edge at $V = 1200\,\mathrm{km\,s^{-1}}$, which would be at $\lambda_2 = 6649$ Å, right in middle of R087 band.

Geometry of bar: in Henney et al. (2005) I pointed out that a diverging cylindrical geometry is necessary to explain the sharp peak in the [N II] emissivity seen at the ionization front. It has been apparent since O'Dell & Yusef-Zadeh (2000) that the nebula contains many bar-like features.

Even for high PDR optical depth, no multiple Raman scattering will occur since the population of $2s$ is very small and the post-scattered photons have insufficient energy to excite any transitions from $1s$.

ACKNOWLEDGMENTS

This work has made use of the Atomic Line List[1] (Van Hoof 2018).

REFERENCES

Bacon, R., Accardo, M., Adjali, L., et al. 2010, in Society of Photo-Optical Instrumentation Engineers (SPIE) Conference Series, Vol. 7735, Proc. SPIE, 773508, doi: 10.1117/12.856027

Bally, J., O'Dell, C. R., & McCaughrean, M. J. 2000, AJ, 119, 2919, doi: 10.1086/301385

Bertoldi, F., & Draine, B. T. 1996, ApJ, 458, 222, doi: 10.1086/176805

Bron, E., Agúndez, M., Goicoechea, J. R., & Cernicharo, J. 2018, arXiv e-prints. https://arxiv.org/abs/1801.01547

Chang, S.-J., Heo, J.-E., Di Mille, F., et al. 2015, ApJ, 814, 98, doi: 10.1088/0004-637X/814/2/98

Clegg, R. E. S., Miller, S., Storey, P. J., & Kisielius, R. 1999, A&AS, 135, 359, doi: 10.1051/aas:1999178

Dopita, M. A., Nicholls, D. C., Sutherland , R. S., Kewley, L. J., & Groves, B. A. 2016, ApJL, 824, L13, doi: 10.3847/2041-8205/824/1/L13

Escalante, V., Sternberg, A., & Dalgarno, A. 1991, ApJ, 375, 630, doi: 10.1086/170225

Greisen, E. W., Calabretta, M. R., Valdes, F. G., & Allen, S. L. 2006, A&A, 446, 747, doi: 10.1051/0004-6361:20053818

Henney, W. J., Arthur, S. J., Williams, R. J. R., & Ferland, G. J. 2005, ApJ, 621, 328, doi: 10.1086/427491

Table 2. Wavelength bands used for Raman wing extraction

	Band	$\langle\Delta\lambda\rangle$, Å	λ_{min}, Å	λ_{max}, Å	$f_{H\alpha}$	$\langle\sigma_\lambda\rangle$, 10^{-21} cm^2	Contamination
Blue wing	B133	−132.8	6414.85	6445.45	0.180	0.144	
	B080	−79.5	6469.25	6496.45	0.196	0.378	Sky 6471, 6478
	B054	−53.6	6499.85	6517.70	0.205	0.802	O II? 6502, 6510, Sky 6507
	B033	−32.8	6518.55	6540.65	0.212	2.069	[N II] 6527.24, [Ni III] 6533.76
Red wing	R040	40.3	6594.20	6611.20	0.238	1.451	Sky 6603
	R058	57.7	6612.05	6628.20	0.244	0.695	
	R087	87.1	6638.40	6660.50	0.255	0.299	[Cr IV]? 6641
	R136	135.7	6688.55	6708.95	0.274	0.119	He I 6699

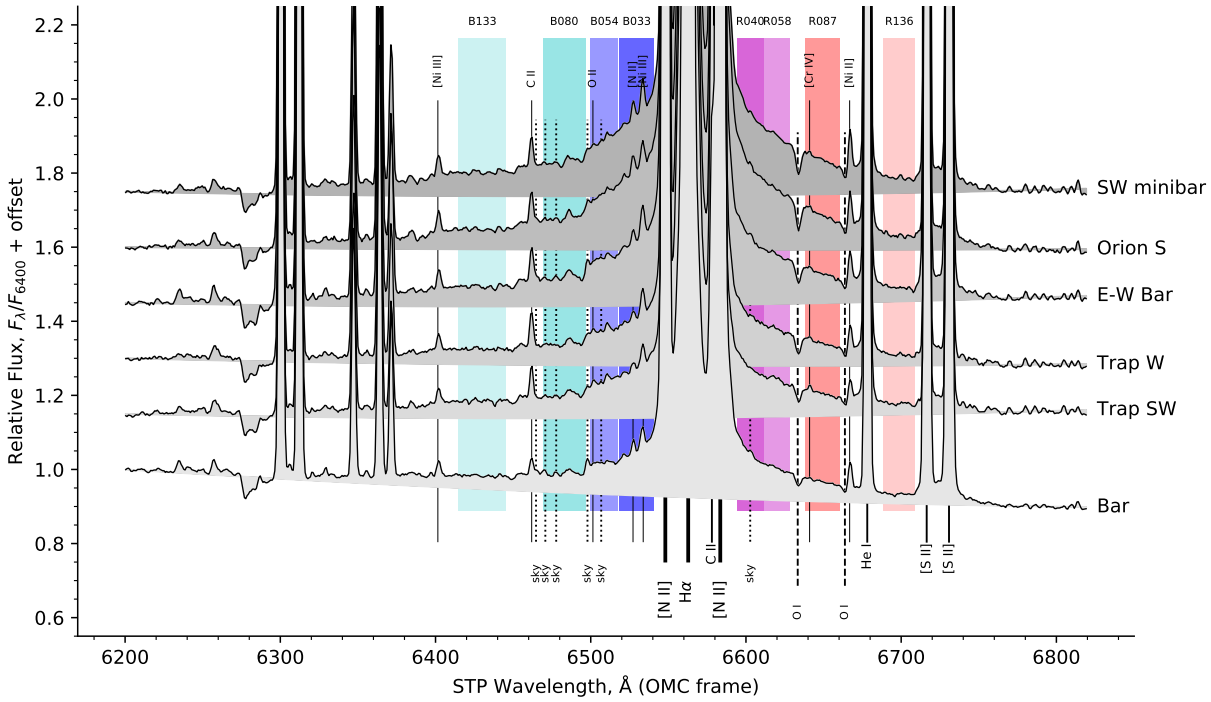

Figure 1. MUSE spectra centered on the Hα line, showing the broad Raman-scattered wings.

Table 3. Fit parameters from Gaussian line fits

	O I			Ni II		
Region	A	V	σ	A	V	σ
A						
B						
C						
D						
E						

Henney, W. J., & O'Dell, C. R. 1999, AJ, 118, 2350, doi: 10.1086/301087

Ivanov, T. I., Salumbides, E. J., Vieitez, M. O., et al. 2008, MNRAS, 389, L4, doi: 10.1111/j.1745-3933.2008.00507.x

Marinov, D., Booth, J. P., Drag, C., & Blondel, C. 2017, Journal of Physics B Atomic Molecular Physics, 50, 065003, doi: 10.1088/1361-6455/aa5a88

Mc Leod, A. F., Weilbacher, P. M., Ginsburg, A., et al. 2015, ArXiv e-prints. https://arxiv.org/abs/1511.01914

Mohr, P. J., Taylor, B. N., & Newell, D. B. 2008, Rev. Mod. Phys., 80, 633, doi: 10.1103/RevModPhys.80.633

Nussbaumer, H., Schmid, H. M., & Vogel, M. 1989, A&A, 211, L27

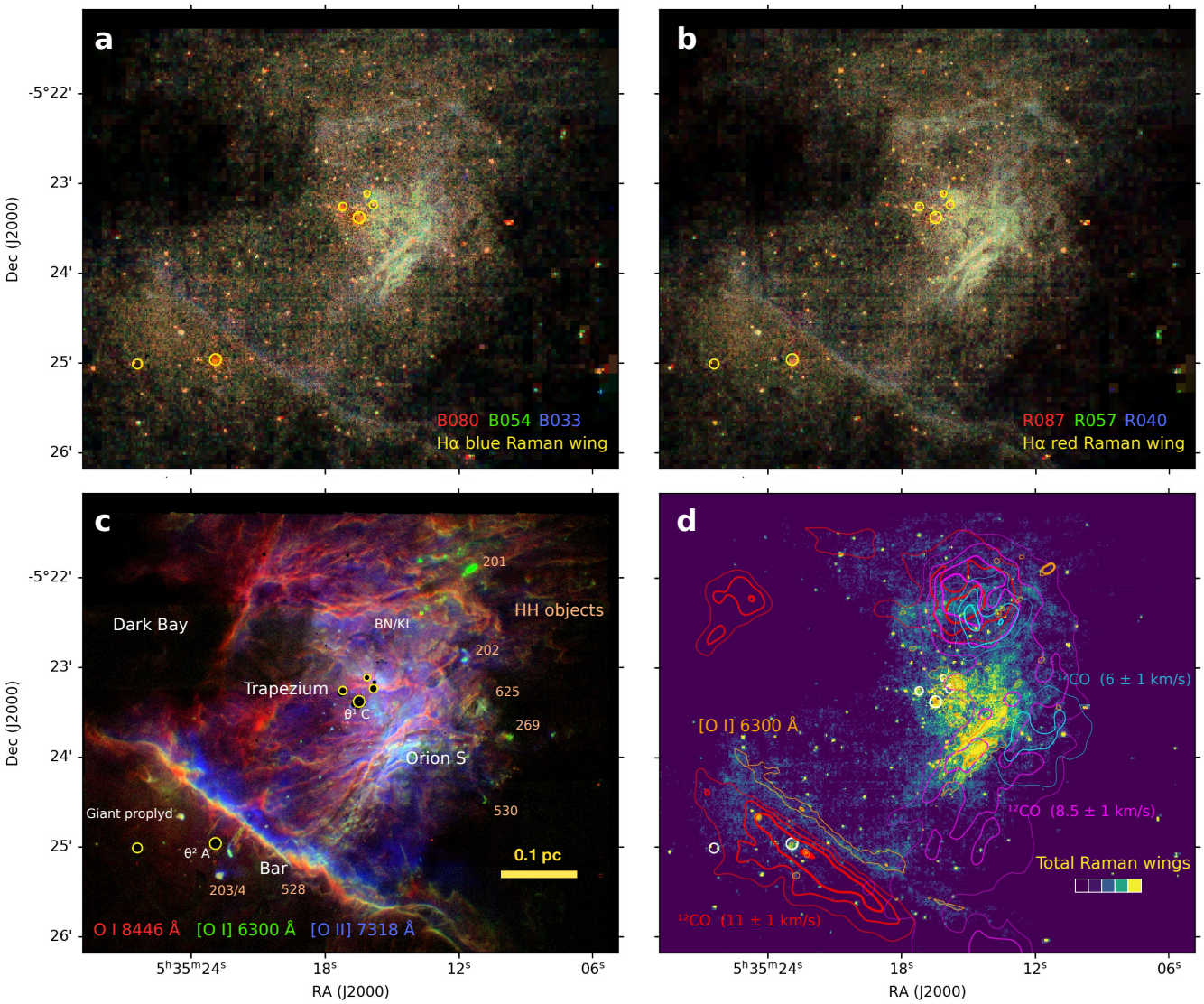

Figure 2. Spatial distribution of Raman-scattered wings in Hα

O'Dell, C. R., & Yusef-Zadeh, F. 2000, AJ, 120, 382, doi: 10.1086/301429

Osterbrock, D. E., & Ferland, G. J. 2006, Astrophysics of gaseous nebulae and active galactic nuclei, 2nd edn. (Sausalito, CA: University Science Books)

Salgado, F., Berné, O., Adams, J. D., et al. 2016, ApJ, 830, 118, doi: 10.3847/0004-637X/830/2/118

Schmid, H. M. 1989, A&A, 211, L31

Stoerzer, H., & Hollenbach, D. 1998, ApJ, 495, 853, doi: 10.1086/305315

Stoerzer, H., Stutzki, J., & Sternberg, A. 1997, A&A, 323, L13

Van Hoof, P. A. M. 2018, Galaxies, 6, doi: 10.3390/galaxies6020063

Watson, A. M., Henney, W. J., & Escalante, V. 1998, in American Astronomical Society Meeting Abstracts, Vol. 193, 16.03

Weilbacher, P. M., Monreal-Ibero, A., Kollatschny, W., et al. 2015, A&A, 582, A114, doi: 10.1051/0004-6361/201526529

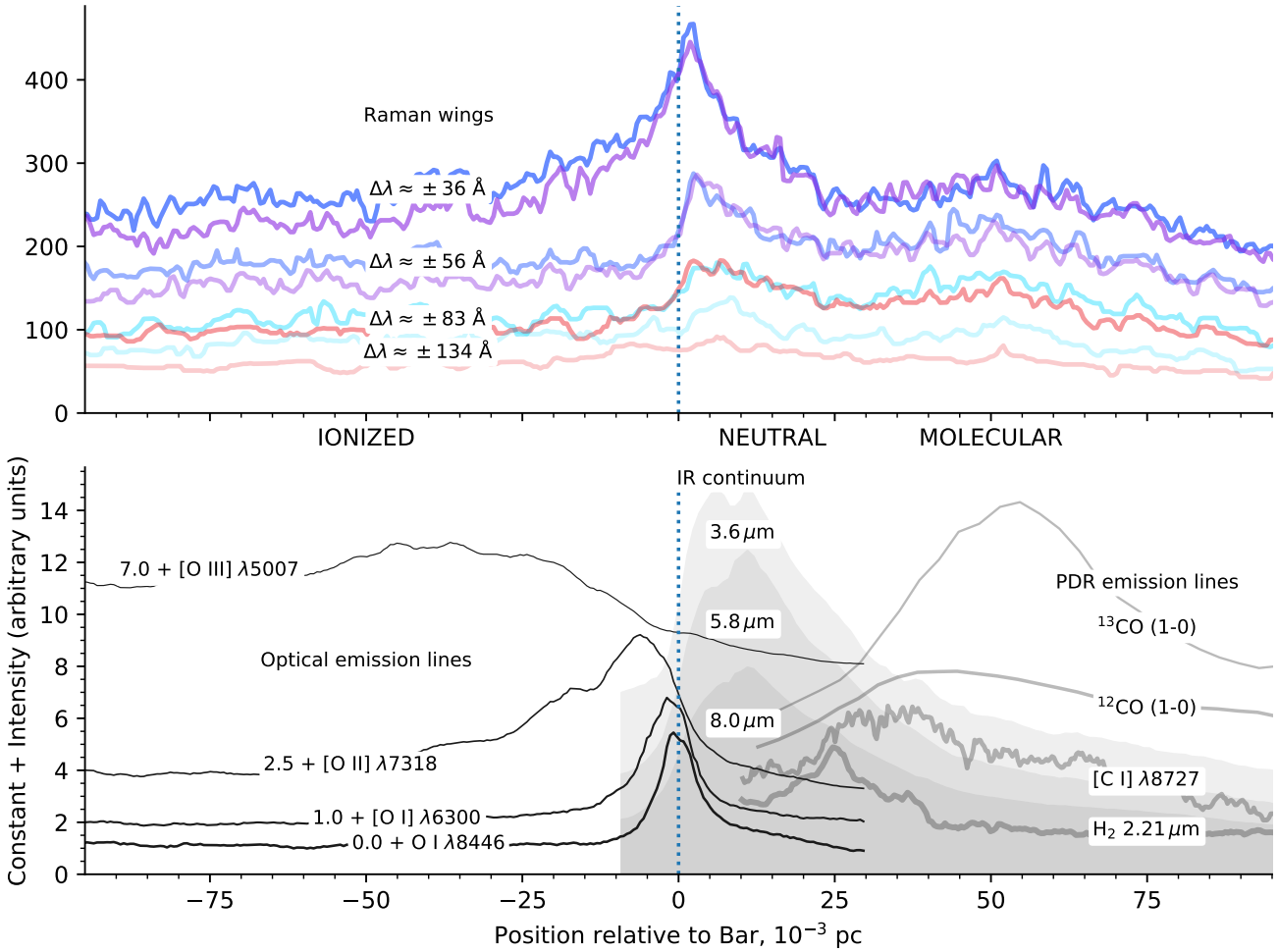

Figure 3. Spatial cut of Raman-scattered Hα wing intensity across the Orion Bar (top panel). Matched red and blue wing bands are shown with color scheme matching Fig. 1.)

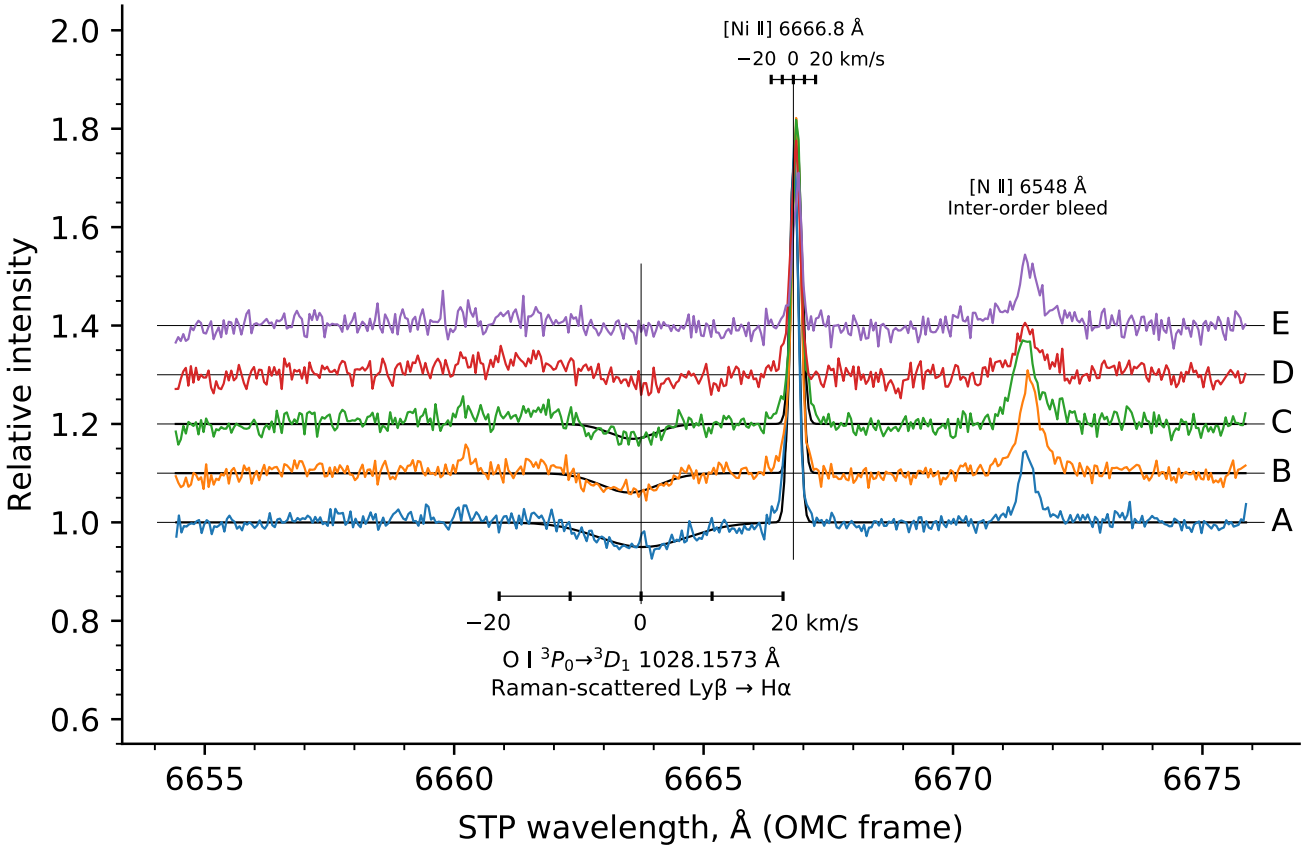

Figure 4. Keck HIRES spectra of Raman-scattered O I absorption line for five regions in Orion South. Wavelengths are given on an air scale and in the rest-frame of the Orion Molecular Cloud, as defined by the peak velocity of ^{13}CO.

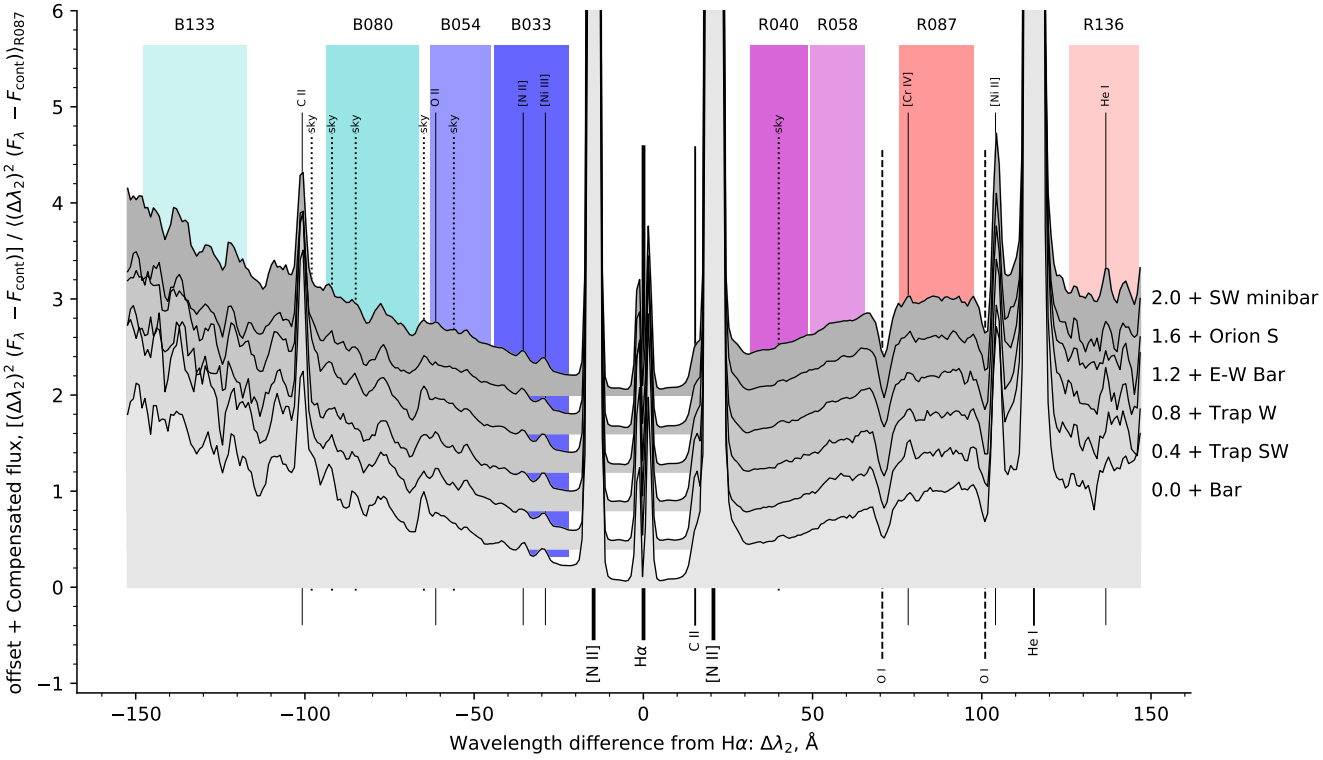

Figure 5. Same as Fig. 1 but with F_λ multiplied by $(\Delta\lambda_2)^2$ and zoomed in on the Raman wing wavelengths. The spectrum is normalized by the average flux in the R087 band and each region is offset vertically by a constant value, as indicated at right. In this presentation, optically thin Raman scattering of a flat FUV spectrum should give a constant value, which for the Orion data is only seen in the R087 and R136 bands.